Asian Journal of Chemistry; Vol. 38, No. 1 (2026), 153-163
ASIAN JOURNAL OF CHEMISTRY
https://doi.org/10.14233/ajchem.2026.34889

Cobalt(III), Nickel(II) and Copper(II) Complexes of Schiff Base Ligand 5-Methoxy-2-[(*E*)-{[2-(thiophen-2-yl)ethyl]imino}methyl]phenol: Synthesis, Characterization, Biological Applications and Docking Studies

R. LATHA[1], G.R. VIJAYAKUMAR[1,*], P.A. SUCHETAN[1], S. SREENIVASA[1], G. SHIVARAJA[2] and B. THIPPESWAMY[3]

[1]Department of Chemistry, University College of Science, Tumkur University, Tumakuru-572103, India
[2]Department of Chemistry, Srinivas University, Institute of Engineering & Technology, Mukka, Mangaluru-574146, India
[3]Department of Chemistry, Maharani's Science College for Women (Autonomous), Mysuru-570005, India

*Corresponding author: E-mail: vijaykumargr18@gmail.com

Received: 13 September 2025 *Accepted*: 17 November 2025 *Published online*: 31 December 2025 AJC-22233

Schiff base ligand, 5-methoxy-2-[(*E*)-{[2-(thiophen-2-yl)ethyl]imino}methyl]phenol (LH) and its cobalt(III), nickel(II) and copper(II) metal complexes *viz.*, $Co(L)_3$, $Ni(L)_2$, $Cu(L)_2$ were synthesized and characterized. The structure of the ligand was established from the X-ray diffraction studies including other conventional techniques *viz.*, FT-IR, UV-visible, ^{1}H NMR, ^{13}C NMR and Mass studies. Complexes of the ligand LH were confirmed through FT-IR, UV-visible and CHN analysis. The ligand (LH) and its metal complexes were evaluated for their antimicrobial and antidiabetic potential, supported by a comprehensive computational molecular docking study. Docking simulations demonstrated strong and favourable binding interactions of the ligand and its complexes with major antimicrobial proteins, DNA gyrase and cytochrome P450 14α-sterol demethylase, as well as antidiabetic targets, α-amylase and α-glucosidase, thereby supporting the experimental findings. The antimicrobial activity was assessed using the agar well diffusion method against bacterial strains *Staphylococcus aureus* and *Escherichia coli*, and fungal strains *Aspergillus flavus* and *Pichia anomala*. Antidiabetic activity was evaluated through *in vitro* α-amylase and α-glucosidase inhibition assays. The results indicated that both the ligand and its metal complexes exhibited moderate to good antibacterial and antifungal activities. However, in antidiabetic studies, the $Cu(L)_2$ complex showed negligible inhibitory activity, while the remaining complexes displayed appreciable effects. Among all the tested compounds, the $Co(L)_3$ complex emerged as the most promising antidiabetic agent, exhibiting significant inhibition of both α-amylase and α-glucosidase enzymes. Overall, the experimental antimicrobial and antidiabetic outcomes showed strong agreement with the molecular docking results, underscoring the reliability of computational predictions in rationalizing the biological behaviour of the synthesized compounds.

Keywords: Schiff base ligand, Metal complexes, Antimicrobial, Antidiabetic activity, Computational molecular docking.

INTRODUCTION

Globally, millions of individuals suffer from serious illnesses like diabetes and bacterial infections. Recently, researchers have looked into the possible application of metal-based compounds as therapeutic tool to address these disorders [1]. Impeding the activity of hydrolytic enzymes intestinal α-glucosidase and pancreatic α-amylase, which are responsible for the conversion of carbohydrates into glucose, is one tactic used to treat diabetes mellitus [2]. This will lower blood glucose levels because it reduces the consumption of dietary carbs and lowers postprandial glycemia [3]. The latest generation of antidiabetic medications such as acarbose, efficiently reduces the intestinal absorption of glucose [4]. Thus, it is necessary to find intriguing antidiabetic medications with exceptional activity and few or no side effects. Likewise, the Gram-positive and Gram-negative pathogenic bacteria are the source of serious infectious diseases that have spread to a global threat level in recent years.

New classes of antibacterial drugs have to be developed to combat infections as a result of the rise in bacteria that are resistant to commonly used antibiotics. In this connection, Schiff bases and their complexes have shown a lot of promise and garnered significant interest from academic researchers from the past two three decades because of their vast variety of physico-chemical properties and varied structural features [5-7]. Compared to other organic ligand based complexes, metal complexes of Schiff bases provide superior modes of

pharmacological action [8,9]. Since the azomethine moiety has nitrogen that is rich in electrons and carbon that is electron-deficient, a variety of electrophilic and nucleophilic reactions could occur at their respective centres [10-13]. Schiff base ligands form a stable metal complex when a functional group, like –OH, is sufficiently near to the azomethine group [8,9,14]. Herein, Schiff base ligand 5-methoxy-2-[(*E*)-{[2-(thiophen-2-yl)ethyl]imino}methyl]phenol (LH) and its cobalt(III), nickel(II) and copper(II) metal complexes were synthesized and screened for their antimicrobial and antidiabetic activities. The ligand (LH) and its metal complexes were also evaluated for their antimicrobial and antidiabetic potential, supported by a comprehensive computational molecular docking study with key antimicrobial (DNA gyrase and cytochrome P450 14α-sterol demethylase) and antidiabetic (α-amylase and α-glucosidase) target proteins.

EXPERIMENTAL

The chemicals and solvents used were procured from S.D. Fine Chemicals, India and were of commercial grade. Ethylamine-2-thiophene and 4-methoxy salicylaldehyde were acquired from Spectrochem, India. TLC silica gel 60 F_{254} plates purchased from Merck Life Science Private Ltd., India was used. Bacterial strains *viz.* Gram-positive *Staphylococcus aureus* MTCC-7443 and the Gram-negative *Escherichia coli* MTCC-7410, the fungal species *Aspergillus flavus* MTCC-9606 and *Pichia anomala* MTCC-237 were purchased from MTCC, Chandigarh, India. Muller Hinton agar media was used for bacteria and Czapek's-Dox agar media was used for fungi.

Characterization: Trimethyl silane (TMS) was used as an internal standard for recording the ^{1}H NMR and ^{13}C NMR spectra of ligand in DMSO-d_6 solvent on a Bruker WM-400 spectrometer (400 MHz). Using a model-Xevo G2-XS QT mass spectrophotometer, ligand mass spectrum was captured. FT-IR analysis was carried out with the Agilent FT-IR spectrophotometer type Cary 630 and spectra were recorded in the range 4000-500 cm^{-1}. Aglient Technologies Cart Eclips UV-visible spectrophotometer was used to record UV-visible spectrum of the samples in the range 200-800 nm. EuroEA Elemental Analyzer was used to perform CHNS analysis of the complexes. Using electrothermal equipment in an open capillary, the melting temperatures of the synthesized ligands and the complexes were ascertained.

Single crystal XRD analysis: A pale yellow, needle shaped single crystal of the LH compound, with dimensions of 0.33 × 0.29 × 0.24 mm^3 was selected and mounted on a Bruker APEX-II CCD diffractometer with monochromated Mo*K*α radiation (λ = 0.71073 Å) at 296(2) K. The data was processed with SAINT and corrected for absorption using SADABS [15]. The structure was solved by the direct method using the program SHELXT and refined by using the program SHELXS-97 [16] by full-matrix least squares technique on F^2 using anisotropic displacement parameters for all non-hydrogen atoms.

Synthesis of 5-methoxy-2-[(*E*)-{[2-(thiophen-2-yl)ethyl]-imino}methyl]phenol (LH): In a 100 mL round-bottom flask, 2-hydroxy-4-methoxybenzaldehyde (0.3043 g, 2 mmol) dissolved in 5 mL ethanol was mixed with thiophene-2-ethylamine (0.254 g, 2 mmol) dissolved in 3 mL of ethanol dropwise followed by the addition of four drops of acetic acid. The reaction mixture was refluxed for 5 h. TLC was used to track the progress of the reaction on a silica gel 60 F_{254} plate with a mobile phase ethyl acetate:petroleum ether (1:1). A clean, needle-like yellow solid that had separated out at the end of the reaction was filtered, cleaned with cold ethanol and dried. The solid product was recrystallized using a 1:1 solvent mixture of heated ethanol and petroleum ether (**Scheme-I**). Dark yellow solid; yield: 82.2%; m.p.: 58-60 ºC; FT-IR (KBr, ν_{max}, cm^{-1}): 3620 (OH), 3026 (C-H aromatic), 2979 (C-H aliphatic), 1633 (C=N), 1545 (C=C aromatic), 1334 (C-N); UV-visible (λ_{max}, nm) 229, 233, 282. ^{1}H NMR (400 MHz, DMSO-d_6, δ ppm): 3.78 (t, *J* = 5.60 Hz, 2H), 3.16 (t, *J* = 6.80 Hz, 2H), 6.96-6.32 (m, 3H), 7.22-7.34 (m, 3H), 8.35 (s, 1H), 13.78 (s, 1H), 3.75 (s, 3H); ^{13}C NMR (DMSO-d_6, δ ppm): 31.202 (C9), 55.703 (C14), 58.436 (C8), 101.496 (C3), 106.23 (C5), 112.368 (C1), 124.686 (C13), 125.948 (C11), 127.408 (C12), 133.663 (C6), 141.910 (C10), 163.774 (C7), 165.685 (C2), 166.069 (C4); Mass (TOF ES+) *m/z*: calcd. (found) %: 262.0684 (261.3394).

Synthesis of metal complexes

[Co(L)$_3$]: $CoCl_2·6H_2O$ (0.119 g, 0.5 mmol) dissolved in 10 mL of methanol was agitated using a magnetic stirrer for 10 min. To a vigorously stirred metal ion solution, a dropwise addition of LH (0.392 g, 1.5 mmol) in methanol (10 mL) was prepared. The stirring was continued further for 2 h. After filtering the resulting brown-red precipitate, it was washed with 10 mL of methanol (three time) followed with 10 mL of diethyl ether (three time) (**Scheme-I**). Brown red solid; yield: 57.1%. Decomposition temperature > 300 ºC. FT-IR (KBr, ν_{max}, cm^{-1}): 3015 (C-H aromatic), 2965 (C-H aliphatic), 1600 (C=N), 1525 (C=C aromatic), 1214 (C-N), 578 (Co-O), 475 (Co-N); UV-Visible (λ_{max}, nm) 200, 290, 445; CHNS data: calcd. (found) % for $C_{42}H_{42}CoN_3O_6S_3$: C, 60.06 (60.01); H, 5.04 (4.99); N, 5.00 (4.92); S, 11.45 (11.39).

[Ni(L)$_2$]: $NiCl_2·6H_2O$ (0.118 g, 0.5 mmol) was dissolved in 10 mL of methanol and agitated using a magnetic stirrer for 10 min. To a vigorously stirred aforementioned solution, a dropwise addition of LH (0.261 g, 1 mmol) in methanol (10 mL) was prepared. The stirring was continued further for 1 h. After filtering the pale green precipitate, it was washed with 10 mL of methanol (three time) followed with 10 mL of diethyl ether (three time) (**Scheme-I**). Pale green solid; yield: 66.1%. Decomposition temperature > 300 ºC. FT-IR (KBr, ν_{max}, cm^{-1}): 3005 (C-H aromatic), 2969 (C-H aliphatic), 1601 (C=N), 1557 (C=C aromatic), 1313 (C-N), 500 (Ni-O), 414 (Ni-N). UV-Visible (λ_{max}, nm) 210, 317, 539; CHNS data: calcd. (found) % for $C_{28}H_{28}N_2NiO_4S_2$: C, 58.05 (57.98); H, 4.87 (4.82); N, 4.84 (4.76); S, 11.07 (11.03).

[Cu(L)$_2$]: $CuSO_4·5H_2O$ (0.12 g, 0.5 mmol) dissolved in 5 mL of methanol was agitated using a magnetic stirrer for 10 min and then added LH (0.26 g, 1 mmol) dropwise in 10 mL of methanol. The stirring was continued further for 1 h. After filtering the green precipitate, it was washed with 10 mL of methanol (three time) followed by 10 mL of diethyl ether (three time) (**Scheme-I**). Green solid; yield: 62.9%; Decom-

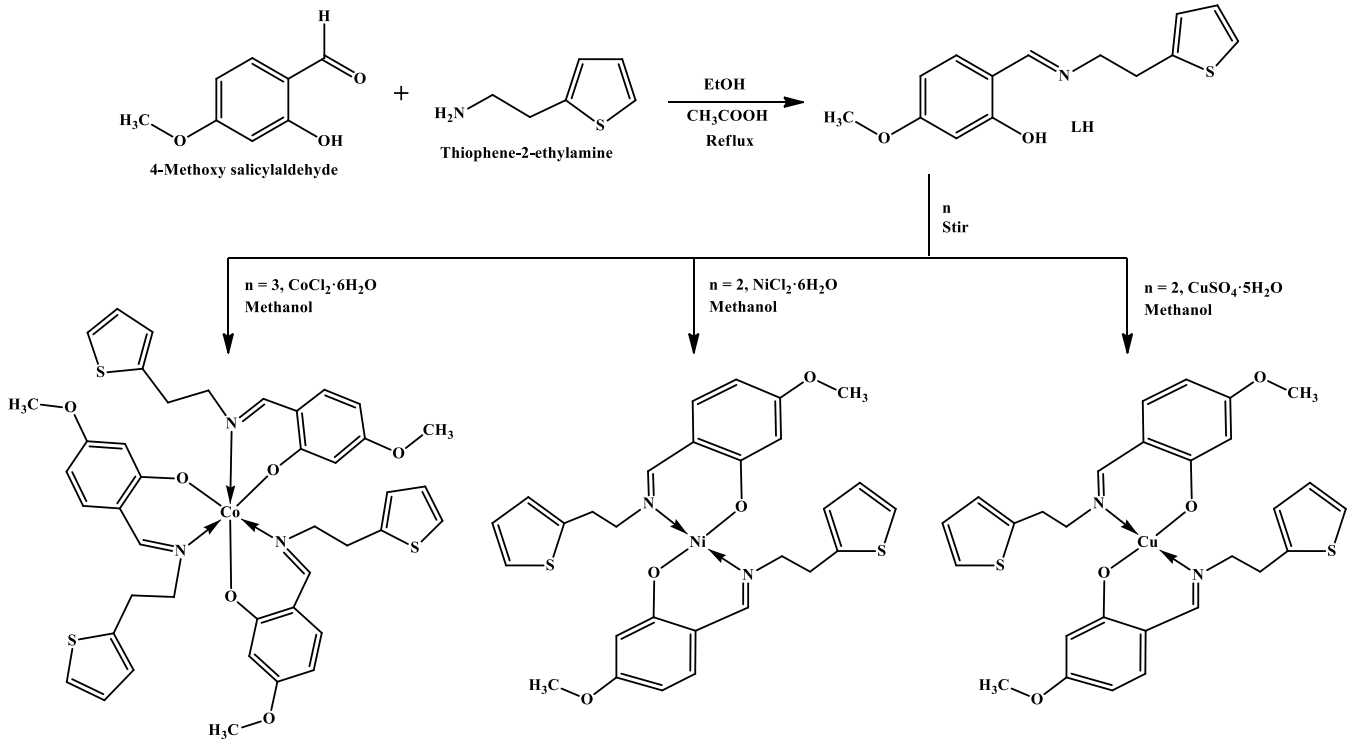

Scheme-I: Synthesis of Schiff base ligand and its metal complexes

position temperature > 300 ºC; FT-IR (KBr, ν_{max}, cm^{-1}): 3021 (C-H aromatic), 2990 (C-H aliphatic), 1602 (C=N), 1530 (C=C aromatic), 1223 (C-N), 504 (Cu-O), 408 (Cu-N); UV-Visible (λ_{max}, nm) 236, 356, 549; CHNS data: calcd. (found) % for $C_{28}H_{28}CuN_2O_4S_2$: C, 57.56 (57.49); H, 4.83 (4.78); N, 4.80 (4.76); S, 10.98 (10.93).

Antimicrobial activity: Slight modifications were made to the agar well diffusion method and was used to evaluate the antibacterial and antifungal activities of the compounds [17]. Two bacterial strains such as Gram-positive *S. aureus* MTCC-7443 and Gram-negative *E. coli* MTCC-7410 and the two fungal strains, *A. flavus* MTCC-9606 and *P. anomala* MTCC-237 were used to test the activity of compounds. The inoculum was adjusted to approximately 5×10^5 CFU/mL with sterile saline solution. Samples were dissolved (10 mg/mL) in DMS as a stock solution and loaded different concentration ranges 100 to 400 µg/mL for different wells. However, for the antifungal activity the concentration ranges from 200 to 800 µg/mL was used. Mueller-Hinton agar was used for the bacterial cultures, while Czapek's-Dox agar medium was employed for fungal species. The bacterial cultures were incubated at 37 ºC for 12-14 h, whereas the fungal cultures were incubated at 28 ºC for 72 h. After incubation, the diameters of the inhibition zones (mm) were measured.

Antidiabetic activity

Inhibitory activity against α-amylase: The α-amylase inhibitory activities of the compounds were assessed as methodology described by Poovitha & Parani [18]. A 100 µL of 0.1 M phosphate buffered saline with pH 6.9 was prepared using porcine pancreatic α-amylase 1 U/mL from SRL, Bangalore, India. Enzyme was pre-incubated with samples at several concentrations (0-100 µg/mL) for 10 min at 37 ºC. By adding substrate (0.1% starch) to the incubation medium, the reaction was started. A 250 µL of 1% 3,5-dinitrosalicylic (DNS) reagent was added to terminate the reaction after 10 min of incubation. The reaction was stopped by maintaining the reaction mixture in a bath of hot water for 10 min. Subsequently, 250 µL of 40% potassium sodium tartrate solution was added. The absorbance at 540 nm was measured following the cooling process to room temperature in a cold-water bath. Using acarbose as a positive control, the percentage of inhibition was determined using the following formula:

$$\text{Inhibition } (\%) = \frac{OD_{Blank} - OD_{Test}}{OD_{Blank}} \times 100$$

The results were represented in IC_{50} values.

Inhibitory activity against α-glucosidase: The procedure outlined in Poovitha & Parani [18] was applied to assess the α-glucosidase inhibitory activities of the samples. In brief, 50 µL of α-glucosidase 1 U/mL from yeast was dissolved in 50 mM, pH 6.9 phosphate buffer and pre-treated individually for 10 min at 37 ºC with varying concentrations of samples (0-100 µg/mL). A 50 µL of 5 mM *p*-nitrophenyl-α-D glucopyranoside in phosphate buffer was added to start the reaction. For 30 min, the enzyme reaction was conducted at 37 ºC. Then, Na_2CO_3 (1 M) was added to stop the reaction and the absorbance at 405 nm was measured. The result was expressed in IC_{50} values in comparison with acarbose as a positive control. The percentage of inhibition was computed using the following formula:

$$\text{Inhibition } (\%) = \frac{OD_{Blank} - OD_{Test}}{OD_{Blank}} \times 100$$

Molecular docking studies: The crystal structures of the target proteins-DNA gyrase (PDB ID: 2XCT), cytochrome P450 14 α-sterol demethylase (PDB ID: 1EA1) and α-amylase (PDB ID: 1OSE), maltase-glucoamylase (PDB ID: 3TOP) were obtained from the Protein Data Bank (http://www.rcsb.org). To prepare these proteins for molecular docking, all water molecules and bound inhibitors were removed. Using Auto-Dock Tools (ADT), polar hydrogens were added, Kolman charges were calculated and the protein structures were converted from PDB to PDBQT format, as required by AutoDock Vina [19].

The chemical structures of compounds [LH, $Co(L)_3$, $Ni(L)_2$ and $Cu(L)_2$] were initially drawn using ChemDraw and subsequently converted to PDB format using Discovery Studio Biovia 2019. These ligand structures were then processed in ADT, where non-polar hydrogens were merged, Kollman charges were assigned and rotatable bonds were defined. Finally, the ligands were saved in PDBQT format, making them compatible with AutoDock Vina.

RESULTS AND DISCUSSION

The ligand LH was initially obtained by the reaction of 4-methoxy salicylaldehyde with thiophene-2-ethylamine by using acetic acid as a catalyst (**Scheme-I**). Ligand LH was recrystallized using ethanol and petroleum ether (1:1) solvent mixture. Ligand structure was confirmed from X-ray diffraction studies and further by using FT-IR, UV-visible, ^{1}H NMR, ^{13}C NMR and mass spectra. The obtained data clearly confirms the formation of Schiff base ligand (LH).

NMR: ^{1}H NMR and ^{13}C NMR spectra were recorded for LH, which clearly confirmed its formation. In the proton NMR spectrum of LH, two methylene groups proton were appeared as triplet in the aliphatic region δ 3.78-3.80 ppm and δ 3.14-3.17 ppm. The methoxy protons were appeared as singlet at δ 3.46 ppm. The aromatic ring protons of benzene ring were appeared at δ 6.96-6.32 ppm and of thiophene were appeared at δ 7.22-7.34 ppm. The azomethine group proton was appears at δ 8.75 ppm. Chemical shift value at δ 13.78 ppm was corresponded to the phenolic -OH and is highly deshielded, due to involving in intramolecular hydrogen bonding with nitrogen [20].

In the ^{13}C NMR spectrum of LH, the azomethine carbon peak was appeared at δ 163.77 ppm [21], C2 carbon peak attached to -OH group was appeared at δ 165.69 ppm and methoxy group attached to C4 position was found at δ 166.07 ppm. These aromatic carbon atoms are deshielded due to attachment to electronegative atoms. The methylene carbon atoms at C8 and C9 were exhibited peaks at δ 58.44 ppm and δ 31.20 ppm, respectively. Four carbon atoms of thiophene ring were appeared at δ 141.90 ppm (C10), 124.69 ppm (C11), 127.41 ppm (C12) and 125.95 ppm (C13). The number of carbon peaks appeared in the spectrum were correlated and confirmed the structure of ligand LH.

Single crystal XRD analysis of LH: The molecular structure of ligand LH is shown in Fig. 1, while its crystal data is given in Table-1. The LH molecule is bent about the C9-C10 bond with the two fragments on each side of the bond being almost planar. The thiophene ring along with attached C10 atom (excluding all H-atoms) is planar with R.M.S.D. of 0.036 (1) Å, while, the phenyl ring with the attached methoxy and hydroxy group and C8=N1-C9 chain (excluding all H atoms) is also planar with R.M.S.D. of 0.023 (1) Å. The planarity of each fragment is further supported by the values of the torsions: C2-C1-C8-N1 = 2.0(7)º, O2-C2-C1-C8 = -2.7(6)º and C3-C4-O1-C7 = 0.0(6)º. The dihedral angle between the two planar segments is 13.7(8)º. The planar conformation is stabilized by intramolecular O2-H2O···N1 hydrogen bond that closes into a ring S(6) motif [16] (Table-2 and Fig. 1).

TABLE-1
CRYSTAL DATA AND STRUCTURE REFINEMENT FOR SCHIFF BASE LIGAND (LH)

CCDC	2323973
Empirical formula	$C_{14}H_{15}NO_2S$
Formula weight	261.33
Temperature (K)	296.15
Crystal system	monoclinic
Space group	$P2_1/c$
a (Å)	12.9714(19)
b (Å)	11.4757(12)
c (Å)	9.2064(10)
β (º)	106.926(9)
Volume (Å)^3	1311.1(3)
Z	4
ρ_{calc} (g/cm^3)	1.324
μ (mm^{-1})	0.240
F(000)	552.0
Crystal size (mm^3)	0.23 × 0.20 × 0.18
Radiation	Mo$K\alpha$ (λ = 0.71073)
2θ range for data collection (º)	3.282 to 55.294
Index ranges	$-16 \le h \le 13$, $-14 \le k \le 13$, $-11 \le l \le 11$
Reflections collected	11312
Independent reflections	2981 [R_{int} = 0.0851, R_{sigma} = 0.0957]
Data/restraints/parameters	2981/4/169
Goodness-of-fit on F^2	1.085
Final R indexes [I>=2σ(I)]	R_1 = 0.0858, wR_2 = 0.2461
Final R indexes [all data]	R_1 = 0.1764, wR_2 = 0.2953
Largest diff. peak/hole/e Å^{-3}	0.55/-0.45

TABLE-2
GEOMETRIC PARAMETERS FOR HYDROGEN BONDS AND OTHER INTERMOLECULAR PARAMETERS OF SCHIFF LIGAND (LH)

D–H···A	D–H	H···A	D···A	D–H/X···A
O2-H2O···N1$^{\#}$	0.82	1.84	2.5858(5)	149
C7-H7A···$\pi^{i, a}$		2.88	3.7394(5)	150
C8-H8···$\pi^{ii, b}$		2.97	3.7562(6)	143
C10-H10B···$\pi^{iii, a}$		2.79	3.7493(5)	172

#: Intra
i: 1-x,-1/2+y,1/2-z; ii: x,1/2-y,1/2+z; iii: x,1/2-y,-1/2+z.
a: Centroid of C11-C12-C13-C14-S1 ring
b: Centroid of C1-C2-C3-C4-C5-C6 ring

The crystal structure does not feature any conventional hydrogen bond and features three C-H···π interactions. Pair of C8-H8···π (involving π-electrons of phenyl ring) and C10-H10B···π (involving π-electrons of thiophene ring) oppositely

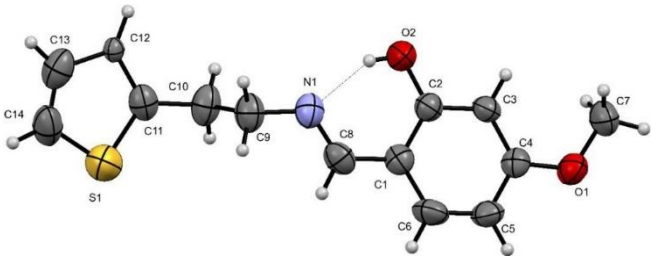

Fig. 1. ORTEP view of molecular structure of Schiff base (LH) ligand. Intramolecular hydrogen bond is shown as a thin line

running chains interconnecting molecules related by c-glide generate a one-dimensional ribbon parallel to *c*-axis (Table-2 and Fig. 2a). The adjacent ribbons related by 2_1 screws (along *b*-axis) are interlinked *via* C7-H7A···π (involving π-electrons of thiophene ring) interactions leading to the formation of a two-dimensional sheet along *bc*-plane (Fig. 2b). Therefore, all the three C-H···π interactions have structure directing features assisting the molecules to ensue 2D sheet like supramolecular architecture.

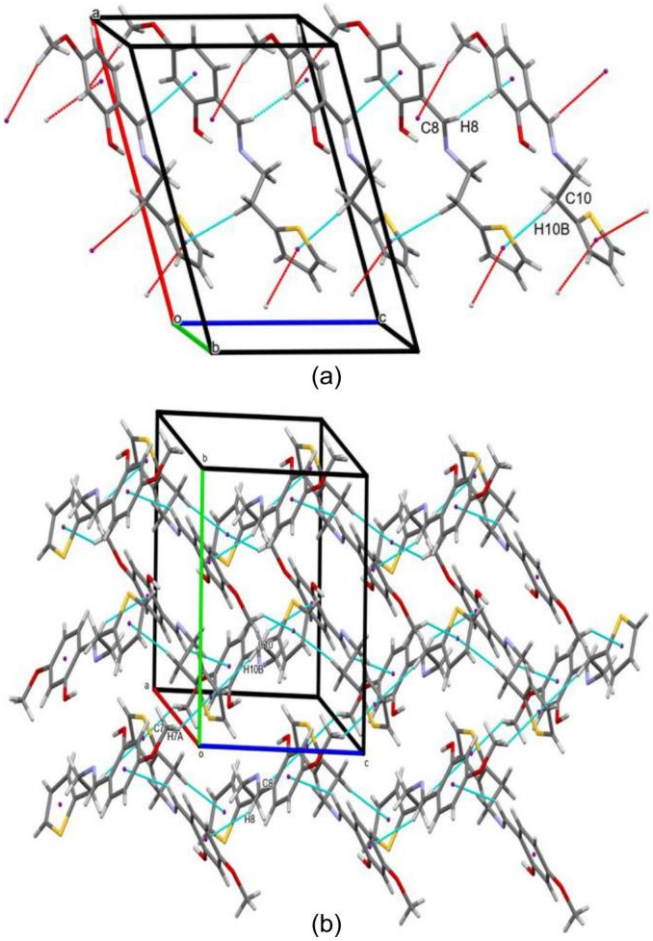

Fig. 2. A partial view of the crystal packing of LH displaying formation of one-dimensional ribbon (a) and two-dimensional sheet (b). Intermolecular interactions are shown as thin blue lines

UV-visible: The UV-visible spectra of ligand and its metal complexes were recorded in distilled water in the range of wavelength 200-800 nm (Fig. 3). In the ligand, the absorption bands appeared at λ_{max} 229 nm and 233 nm are due to the π-π* transition of aromatic ring. The band absorbed at λ_{max} 282 nm was attributed to the charge transfer transition within the delocalized π-system [21]. While in the Co(III) and Ni(II) complexes, the absorption bands observed respectively at λ_{max} 200 nm and 210 nm were attributed to π-π* transition of coordinated ligand. In the same complexes, the absorption bands at λ_{max} 290 nm and 317 nm were due to n-π* transition. The bands at λ_{max} 445 nm in $Co(L)_3$ and 539 nm in $Ni(L)_2$ were due the ligand to metal charge transfer spectra (LMCT). The Cu(II) complexes belong d^9 system, the absorption band appeared at 236 nm was due to π–π* transition, 356 nm was due to n-π* transition and at 549 nm could be assigned to square planar $^2A_{1g} \rightarrow {}^2B_{1g}$ transition [22].

FT-IR: The infrared spectrum of the ligand exhibited a peak at 3620 cm^{-1}, corresponding to the –OH group of the Schiff base ligand (LH) (Fig. 4a). This band was absent in the corresponding metal complexes, indicating deprotonation of the phenolic group and coordination of the resulting phenoxide ion to the metal center. Another prominent peak appears at 1633 cm^{-1} was clearly indicates the formation of azomethine group in the ligand. In the metal complexes, the same peak position was reduced to lower wavenumber region of about ~30 cm^{-1}. This confirms that the nitrogen atom of the azomethine (HC=N-) group was involved in bond formation with the respective metal atoms. The peaks observed in LH and its Co(III), Ni(II) and Cu(II) metal complexes between 1557-1525 cm^{-1} were corresponded to the aromatic C=C stretching vibration. The coordinated C-O vibration which appeared at 1291 cm^{-1} in free ligand was undergo red-shift due to the participation in bonding. The metal bonding with nitrogen atom appears at 475 cm^{-1}, 414 cm^{-1} and 408 cm^{-1} for Co(III), N(II) and Cu(II) complexes, respectively, whereas the metal bonding with oxygen atom (M-O) appears respectively at 578 cm^{-1}, 500 cm^{-1} and 504 cm^{-1} (Fig. 4b-d) [23].

Antimicrobial activity: The agar well diffusion method was used to examine the antimicrobial activity of Schiff base ligand (LH) and its cobalt(III), nickel(II) and copper(II) metal complexes against a bacterial strains Gram-positive *S. aureus* MTCC-7443 and Gram-negative *E. coli* MTCC-7410. Also, antifungal activity against two fungus species, *A. flavus* MTCC-9606 and *P. anomala* MTCC-237, was investigated. Significant activity was demonstrated by the synthesized LH ligand and its metal complexes against tested bacteria and fungi. In general, the predominant activity was observed at sample concentrations of 800 μg/mL for antifungal activity and 400 μg/mL for antibacterial activity. Among the synthesized compounds the $Co(L)_3$ showed good antibacterial activity against both *S. aureus*, with a zone of inhibition (mm) 12.33 ± 0.57 and *E. coli* with a zone of inhibition (mm) 12.66 ± 0.57. Among all the tested compounds, the Schiff base ligand LH showed good antifungal activity against both *A. flavus* and *P. anomala* with a zone of inhibition (mm) 22.33 ± 2.08 and 15.33 ± 0.5, respectively. It has been evidenced that antifungal activity decreases on complexation (Table-3).

Antidiabetic activity

α-Amylase and α-glucosidase inhibition activity: The synthesized compounds were screened to evaluate the inhibition activity against α-amylase and α-glucosidase enzymes.

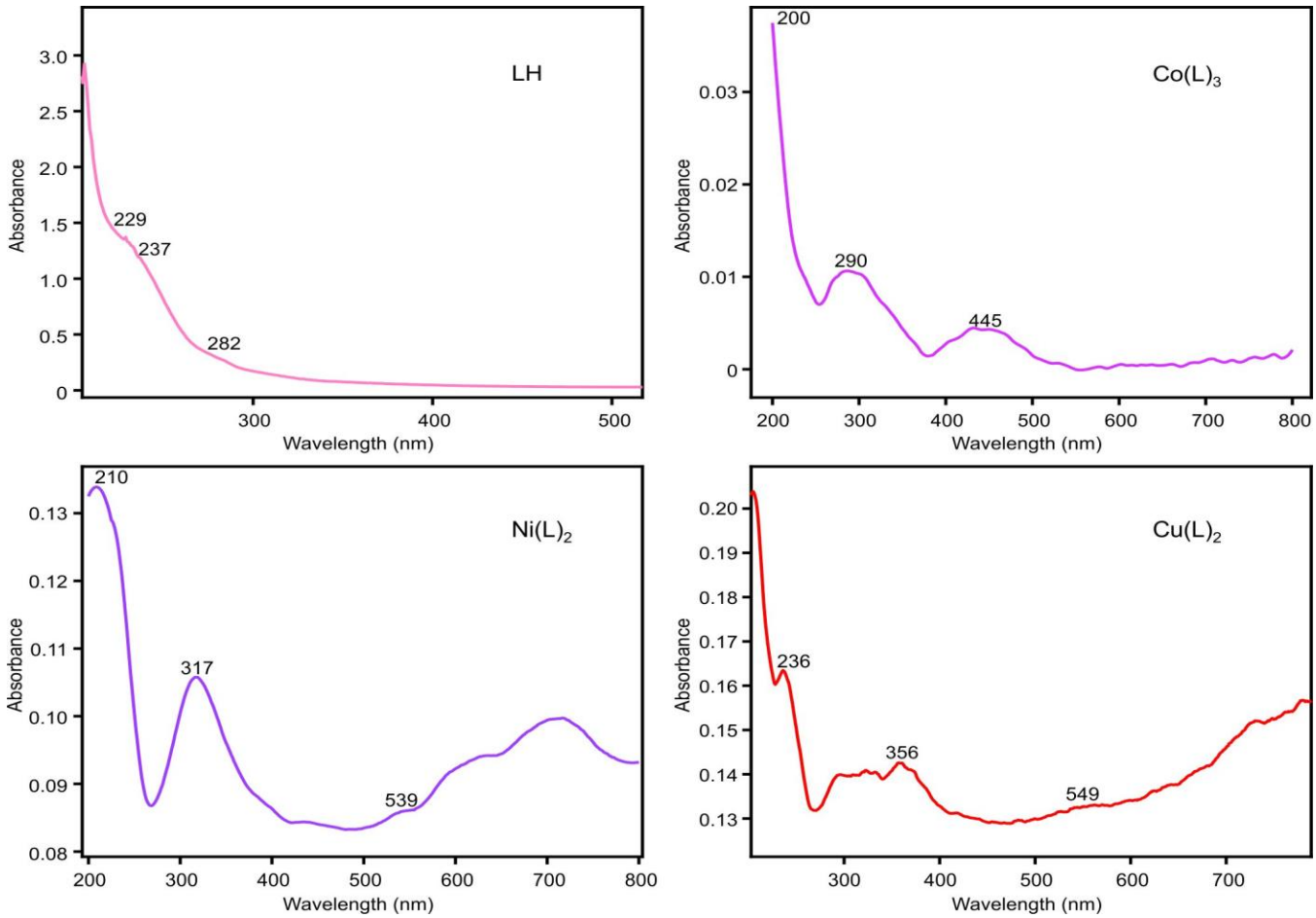

Fig. 3. Electronic spectra of Schiff base ligand (LH) and its Co(III), Ni(II) and Cu(II) complexes

TABLE-3
ANTIMICROBIAL ACTIVITY DATA OF SCHIFF BASE LIGAND (LH) AND ITS Co(III), Ni(II) AND Cu(II) METAL COMPLEXES

Compound	Bacterial strains	Concentration (µg/mL)			
		100	200	300	400
LH	*S. aureus*	–	–	8.33 ± 0.57	11.66 ± 1.15
	E. coli	–	–	9.33 ± 0.57	11.33 ± 1.15
$Co(L)_3$	*S. aureus*	–	–	7.66 ± 1.52	12.33 ± 0.57
	E. coli	–	–	–	12.66 ± 0.57
$Ni(L^2)_2$	*S. aureus*	–	–	–	11.33 ± 0.57
	E. coli	–	–	5.33 ± 0.57	11.66 ± 0.57
$Cu(L)_2$	*S. aureus*	–	–	–	9.33 ± 0.57
	E. coli	–	–	6.33 ± 0.57	6.66 ± 0.57
Standard**	*S. aureus*	13.33 ± 0.57	15.33 ± 0.57	18.33 ± 0.57	20.66 ± 0.57
	E. coli	16.33 ± 1.15	19.66 ± 0.57	21.33 ± 0.57	22.66 ± 0.57
Compound	Fungal strains	Concentration (µg/mL)			
		200	400	600	800
LH	*A. flavus*	–	–	16.66 ± 0.57	22.33 ± 2.08
	P. anomala	–	–	12.33 ± 0.57	15.33 ± 0.57
$Co(L)_3$	*A. flavus*	–	–	–	18.33 ± 0.57
	P. anomala	–	–	–	12.66 ± 057
$Ni(L^2)_2$	*A. flavus*	–	–	–	14.66 ± 1.15
	P. anomala	–	–	–	12.33 ± 0.57
$Cu(L)_2$	*A. flavus*	–	–	–	11.33 ± 0.57
	P. anomala	–	–	–	11.33 ± 0.57
Standard**	*A. flavus*	–	10.66 ± 1.52	15.66 ± 0.57	21.66 ± 1.52
	P. anomala	–	10.66 ± 0.57	15.33 ± 0.57	19.66 ± 1.52

**In place of the current sample concentrations, standard kanamycin in the concentration range of 20, 40, 60 and 80 µg/mL for antibacterial activity and standard fluconazole in the concentration range of 100, 200, 400 and 600 µg/mL for antifungal activity were used.
± denotes the standard deviation value.

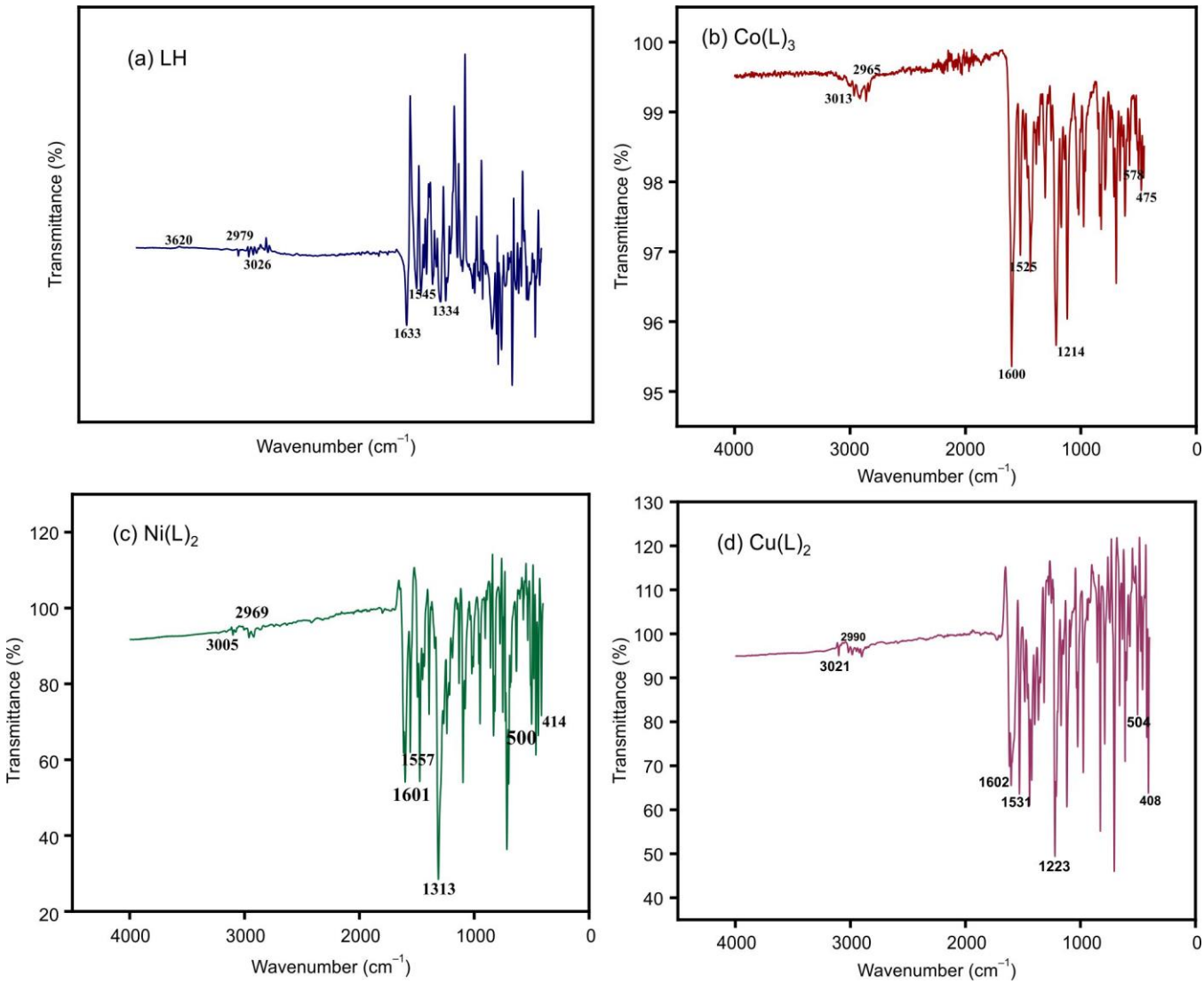

Fig 4. FT-IR spectra of (a) Schiff base ligand (LH), and its (b) $Co(L)_3$, (c) $Ni(L)_2$, (d) $Cu(L)_2$ complexes

The % of inhibition of both enzymes with respect to concentration in μg/mL were represented through the graphs (Fig. 5), which clearly indicates that as the concentration of compounds increases the percentage of inhibition activity also increases. The obtained IC_{50} (μg/mL) values for α-amylase and α-glucosidase enzymes are also shown in Fig. 5. Among the synthesized compounds cobalt complex, $Co(L)_3$ showed good antidiabetic activity when compared to ligand and other synthesized metal complexes. The IC_{50} (μg/mL) value for this complex against α-glucosidase was 73.106 and against α-amylase was 137.181. The enhanced activity for this complex may be due to the binding effects of the coordinated ligand as well as the metal with the studied enzymes. Further azomethine group of the coordinated ligand is also responsible for exhibiting the good antidiabetic activity.

Molecular docking studies: The Schiff base ligand LH and its metal complexes $Co(L)_3$, $Ni(L)_2$ and $Cu(L)_2$ were docked into the active sites of several target proteins *viz*. DNA gyrase (PDB ID: 2XCT), cytochrome P450 14α-sterol demethylase (PDB ID: 1EA1), α-amylase (PDB ID: 1OSE) and maltase-glucoamylase (PDB ID: 3TOP).

All the tested compounds showed favourable binding energies, ranging from -6.8 to -10.2 kcal/mol (Table-4). In general, the metal complexes exhibited stronger binding affinities than the parent ligand LH. Notably, the $Co(L)_3$ complex demonstrated robust docking scores of -6.8 kcal/mol against DNA gyrase (2XCT) and -10.2 kcal/mol against P450 demethylase (1EA1), in excellent agreement with the antimicrobial assays. Similarly, $Ni(L)_2$ achieved strong binding energies of -8.6 kcal/mol (2XCT) and -10.2 kcal/mol (1EA1). Moreover, the $Co(L)_3$-2XCT complex revealed the multiple hydrogen-bonding interactions: a conventional H-bond with Gly584 and non-conventional H-bonds with His1081, Glu435 and Asp510. In the $Co(L)_3$–1EA1 complex, a significant H-bond with Arg96 was observed. Furthermore, pi–cation, pi–anion and π–π stacking interactions were also detected (Table-4), reinforcing the strong binding profiles of the metal complexes (Fig. 6).

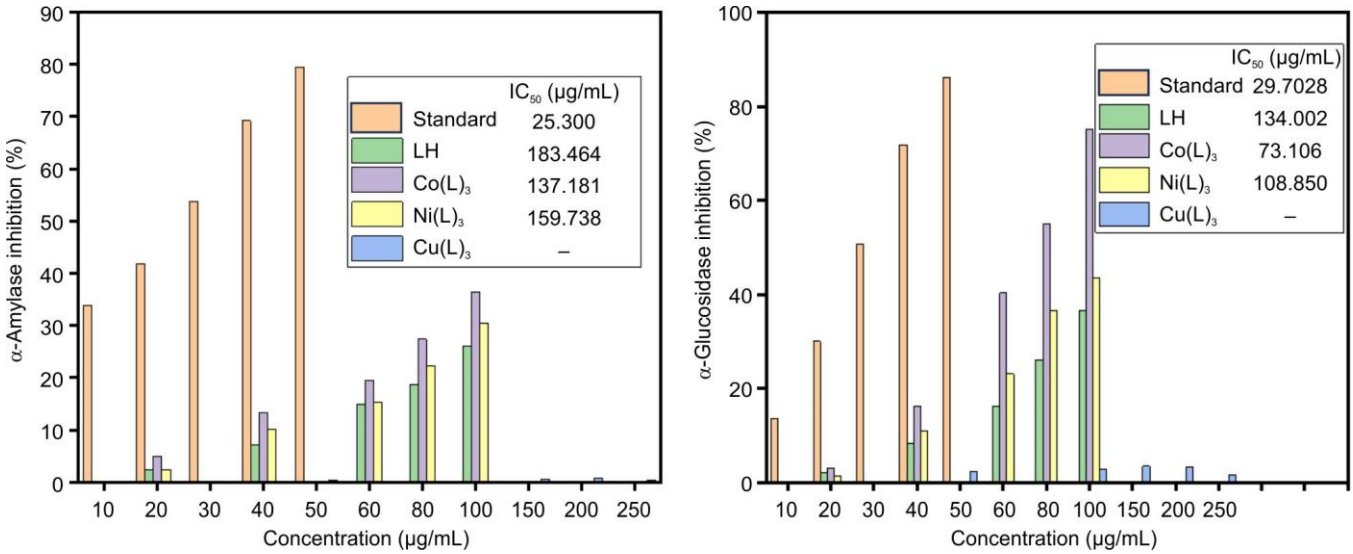

Fig. 5. α-Amylase and percentage α-glucosidase inhibition activity (%) and IC_{50} (μg/mL) values for Schiff base and its metal complexes

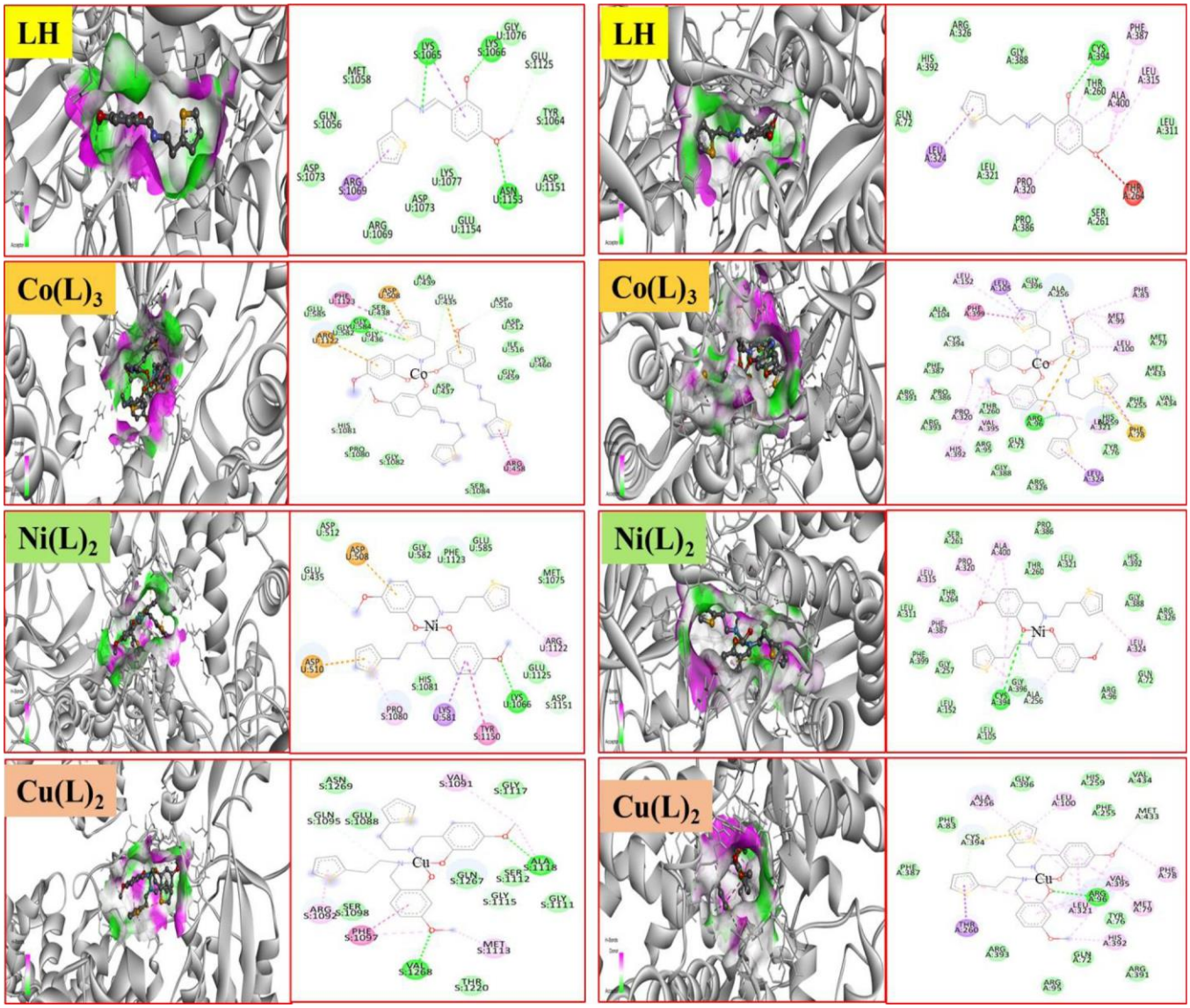

Fig. 6. Binding poses of Schiff base (LH) and its $Co(L)_3$, $Ni(L)_2$ and $Cu(L)_2$ complexes with target proteins 2XCT and 1EA1

TABLE-4
MOLECULAR INTERACTIONS OF TARGET MOLECULES (SCHIFF BASE (LH) AND ITS $Co(L)_3$, $Ni(L)_2$, $Cu(L)_2$ COMPLEXES) WITH TARGET PROTEIN PDB ID 2XCT AND PDB ID 1EA1

Ligands	Docking energy (Kcal/mol)		Interacted active site residues	
	2XCT	1EA1	2XCT	1EA1
LH	-6.8	-7.1	Lys1065 (hydrogen bond), Lys1065 (H bond), Lys1066 (H bond), Asn1153 (H bond), Glu1125 (H bond), Lys1065 (Pi-sigma), Arg1069 (Pi-sigma).	Cys394 (H bond), Leu324 (Pi-sigma), Ala400 (alkyl), Leu315 (alkyl), Phe387 (Pi-alkyl), Pro320 (Pi-alkyl), Cys394 (Pi-alkyl), Ala400 (Pi-alkyl).
$Co(L)_3$	-6.8	-10.2	Gly584 (H bond), His1081 (NC H bond), Glu435 (NC H bond), Asp510 (NC H bond), Arg1122 (Pi-cation), Glu435 (Pi-anion), Asp508 (Pi-anion), Phe1123 (Pi-Pi staked), Arg458; Gly459 (amide Pi-staked), Arg458 (Pi-alkyl).	Arg96 (H bond), Ala256 (NC H bond), Arg96 (Pi-cation), Arg96 (Pi-donor), Cys394 (Pi-donor H bond); Leu105 (Pi-sigma), Ala256 (Pi-sigma), Leu324 (Pi-sigma), Phe78 (Pi-sulfur), Phe399 (Pi-Pi T-shaped), Phe78 (Pi-Pi T-shaped), Leu100 (alkyl), Val395 (alkyl), Pro320 (alkyl), Leu321 (alkyl), Met99 (Pi-alkyl), Phe83 (Pi-alkyl), His392 (Pi-alkyl), Arg96 (Pi-alkyl), Leu152 (Pi-alkyl), Ala256 (Pi-alkyl), Leu100 (Pi-alkyl), Leu321 (Pi-alkyl).
$Ni(L)_2$	-8.6	-10.2	Lys1066 (H bond), Glu435 (NC H bond), Asp1151 (NC H bond), Asp508 (Pi-anion), Asp510 (Pi-anion), Lys581 (Pi-sigma), Tyr1150 (Pi-Pi T-shaped), Pro1080 (Pi-alkyl), Arg1122 (Pi-alkyl).	Cys394 (H bond), Ala256 (NC bond), Ala400 (Pi-sulfur), Leu315 (alkyl), Phe387 (alkyl), Pro320 (Pi-alkyl), Cys394 (Pi-alkyl), Ala400 (Pi-alkyl), Ala256 (Pi-alkyl), Leu324 (Pi-alkyl), Ala256 (Pi-alkyl).
$Cu(L)_2$	-8.1	-8.5	Ala1118 (H bond), Val1268 (H bond), Gly1115 (NC H bond), Gln1095 (NC H bond), Phe1097 (Pi-Pi T-shaped), Ala1118 (alkyl), Met1113 (alkyl), Val1091 (alkyl), Phe1097 (Pi-alkyl), Arg1092 (Pi-alkyl).	Arg96 (H bond), Met433 (NC H bond), Cys394 (Pi-donor H bond), Thr260 (Pi-sigma), Cys394 (Pi-sulfur),Val395 (alkyl), Leu321 (alkyl), Phe78 (Pi-alkyl), His392 (Pi-alkyl), Arg96 (Pi-alkyl), Val395 (Pi-alkyl), Met79 (Pi-alkyl), Leu321 (Pi-alkyl), Leu321 (Pi-alkyl), Arg96 (Pi-alkyl), Leu100 (Pi-alkyl), Ala256 (Pi-alkyl), Val395 (Pi-alkyl).

For antidiabetic docking studies, α-amylase (PDB ID: 1OSE) and maltase-glucoamylase (α-glucosidase; PDB ID: 3TOP) were selected as targets due to their crucial roles in the sequential breakdown and absorption of dietary carbohydrates. α-Amylase initiates starch hydrolysis by cleaving α-1,4 glycosidic bonds into oligosaccharides, while α-glucosidase further converts these smaller sugars into absorbable glucose, both actions directly influencing post-prandial blood glucose levels. Docking simulations of the ligand LH and its metal complexes against these proteins showed binding energies in the range of -6.7 to -8.5 kcal/mol as shown in Table-5. Among the complexes, $Co(L)_3$ displayed notable binding affi-

TABLE-5
MOLECULAR INTERACTIONS OF TARGET MOLECULES (SCHIFF BASE (LH) AND ITS $Co(L)_3$, $Ni(L)_2$, $Cu(L)_2$ COMPLEXES) WITH TARGET PROTEIN PDB ID 1OSE AND 3TOP

Ligands	Docking energy (Kcal/mol)		Interacted active site residues	
	1OSE	3TOP	1OSE	3TOP
LH	-6.7	-6.7	Lys200 (H bond), Glu233 (H bond), Ala198 (NC H bond), Asp197 (NC H bond), His201 (Pi-cation), Ile235 (Pi-sigma), Tyr62 (Pi-Pi stacked), His201 (Pi-Pi T-shaped), Ile235 (alkyl), Lys200 (Pi-alkyl).	Arg1510 (H bond), Asp1526 (H bond), Asp1420 (NC H bond), Asp1526 (Pi-anion), Trp1369 (Pi-Pi stacked), Trp1369 (Pi-Pi stacked), Tyr1251 (Pi-Pi T-shaped), Trp1355 (Pi-Pi T-shaped), Phe1559 (Pi-Pi T-shaped), Ile1315 (alkyl), Trp1418 (Pi-alkyl).
$Co(L)_3$	-6.7	-4.6	Arg398 (NC H bond), Asp402 (NC H bond), Asp402 (Pi-anion), Ser289 (Pi-donor hydrogen bond), Arg398 (alkyl), Pro4 (Pi-alkyl), Pro332 (Pi-alkyl).	Gln1227 (H bond), His1639 (NC H bond), Glu1629 (NC H bond), Glu1231 (Pi-anion), Leu1224 (Pi-sigma), Leu1224 (Pi-sigma), Pro1220 (alkyl), Leu1224 (alkyl), Pro1658 (Pi-alkyl).
$Ni(L)_2$	-8.5	-8.2	His201 (Pi-cation), His305 (Pi-sulfur), His305 (Pi-Pi stacked), Tyr62 (Pi-Pi stacked), His305 (Pi-Pi T-shaped), Lys200 (Pi-alkyl), Ile235 (Pi-alkyl), Trp59 (Pi-alkyl), Trp59 (Pi-alkyl), His201 (Pi-alkyl), His305 (Pi-alkyl), Val163 (alkyl), Leu162 (alkyl).	Lys1460 (H bond), Asp1526 (Pi-anion), Trp1369 (Pi-sulfur), Trp1369 (Pi-Pi Staked), Trp1369 (Pi-Pi stacked), Trp1355 (Pi-Pi T shaped), Phe1559 (Pi-Pi T shaped), Trp1369 (Pi-alkyl), Trp1369 (Pi-alkyl), Phe1559 (Pi-alkyl), His1584 (Pi-alkyl), Ile1587 (Pi-alkyl), Pro1159 (Pi-alkyl).
$Cu(L)_2$	-8.0	-7.3	His201(H bond), Glu233 (NC H bond), Glu233 (NC H bond), His305 (Pi-cation), Asp197 (Pi-anion), Trp59 (Pi-sigma), His305 (Pi-Pi stacked), Trp59 (Pi-Pi T-shaped), His305 (Pi-Pi T-shaped), Ile235 (Pi-alkyl), Trp59 (Pi-alkyl), His201 (alkyl), Val163 (Pi-alkyl), Ala198 (Pi-alkyl).	Trp1369 (H bond), Lys1460 (H bond), Trp1369 (Pi-Pi stacked), Trp1369 (Pi-Pi stacked), Trp1355 (Pi-Pi T shaped), Lys1460 (alkyl), Tyr1251 (Pi-alkyl), Trp1355 (Pi-alkyl), Trp1369 (Pi-alkyl), Pro1159 (Pi-alkyl).

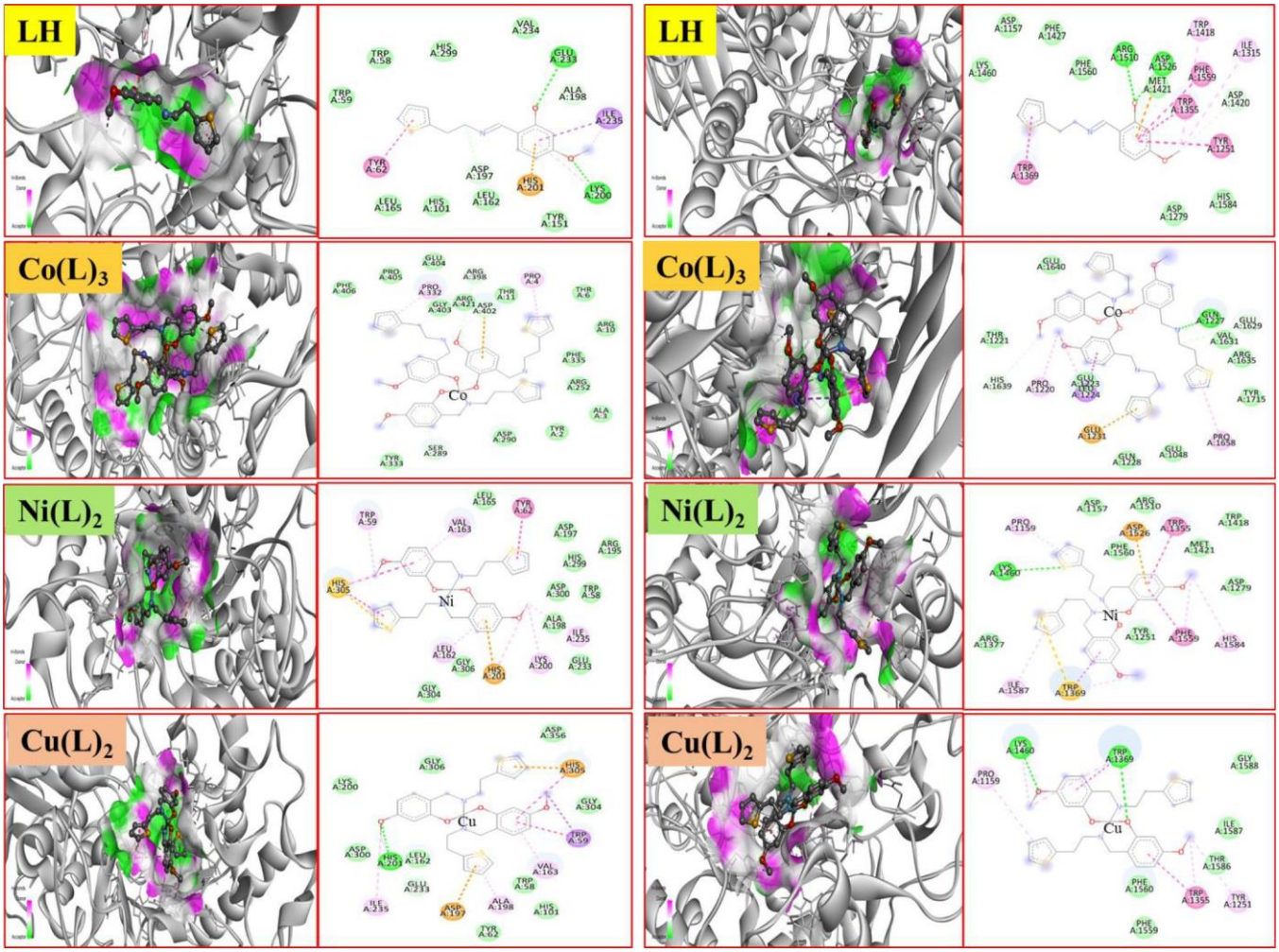

Fig. 7. Binding poses of Schiff base (LH) and Its $Co(L)_3$, $Ni(L)_2$, $Cu(L)_2$ complexes with target proteins 1OSE and 3TOP

nities of -6.7 kcal/mol with α-amylase (1OSE) and -4.6 kcal/mol with maltase-glucoamylase (3TOP). Importantly, the $Co(L)_3$–3TOP complex formed a hydrogen bond with Gln-1227, accompanied by several other stabilizing non-covalent contacts across the active site (Fig. 7).

Conclusion

The synthesis, characterization, antibacterial, antifungal and antidiabetic activities of Schiff base ligand 5-methoxy-2-[(*E*)-{[2-(thiophen-2-yl)ethyl]imino}methyl]phenol (LH) and its Co(III), Ni(II) and Cu(II) metal complexes are reported. Nickel(II) and copper(II) ions formed four-coordinated complexes whereas the cobalt formed the six-coordinated complex with Schiff base ligand LH. With respect to antimicrobial activities of the ligand and its complexes, $Co(L)_3$ showed significant anti-bacterial activity against *S. aureus* and *E. coli* bacteria whereas ligand LH showed good antifungal activity against *A. flavus* and *P. anomala*. With regard to antidiabetic activity, the complex $Co(L)_3$ reveals good antidiabetic activity against both α-amylase and α-glucosidase. The obtained results were correlated with the results obtained from molecular docking. It is concluded that Schiff base ligand LH and its Co(III), Ni(II) and Cu(II) metal complexes become prominent antimicrobial and antidiabetic agents.

ACKNOWLEDGEMENTS

The authors are thankful to the Tumkur University for their support and encouragement.

CONFLICT OF INTEREST

The authors declare that there is no conflict of interests regarding the publication of this article.

DECLARATION OF AI-ASSISTED TECHNOLOGIES

During the preparation of this manuscript, the authors used an AI-assisted tool(s) to improve the language. The authors reviewed and edited the content and take full responsibility for the published work.

REFERENCES

1. H.O. Omoregie, T.L. Yusuf, S.D. Oladipo, K.A. Olofinsan, M.B. Kassim and S. Yousuf, *Polyhedron*, **217**, 115738 (2022); https://doi.org/10.1016/j.poly.2022.115738
2. M. Taha, T. Noreen, S. Imran, F. Nawaz, S. Chigurupati, M. Selvaraj, F. Rahim, N.H. Ismail, A. Kumar, A. Mosaddik, A.M. Alghamdi, Y.A.N. Alqahtani and A.A.N. Alqahtani, *Med. Chem. Res.*, **28**, 2010 (2019); https://doi.org/10.1007/s00044-019-02431-4

3. T. Matsui, T. Tanaka, S. Tamura, A. Toshima, K. Tamaya, Y. Miyata, K. Tanaka and K. Matsumoto, *J. Agric. Food Chem.*, **55**, 99 (2007); https://doi.org/10.1021/jf0627672
4. S. Zhang and S.M. Kim, *Appl. Organomet. Chem.*, **33**, 5102 (2019); https://doi.org/10.1002/aoc.5102
5. G. Vinita, S. Sanchita and Y.K. Gupta, *Res. J. Chem. Sci*, **2231**, 606X (2013).
6. G. Venkatesh, P. Vennila, S. Kaya, S.B. Ahmed, P. Sumathi, V. Siva, P. Rajendran and C. Kamal, *ACS Omega*, **9**, 8123 (2024); https://doi.org/10.1021/acsomega.3c08526
7. S. Thakur, A. Jaryal and A. Bhalla, *Results Chem.*, **7**, 101350 (2024); https://doi.org/10.1016/j.rechem.2024.101350
8. E. Uddin, M.N. Sardar, M.S. Reza, M.S. Hasan, M.T. Talukder, M.M. Hoque, P. Paul, Mst. S. Khatun, M.F. Hossen, M.A. Asraf and M. Kudrat-E-Zahan, *Discov. Chem.*, **2**, 153 (2025); https://doi.org/10.1007/s44371-025-00228-6
9. P. Singh, P. Yadav, K.K. Sodhi, A. Tomer and S.B. Mehta, *Results Chem.*, **7**, 101222 (2024); https://doi.org/10.1016/j.rechem.2023.101222
10. D.S. Timofeeva, A.R. Ofial and H. Mayr, *Tetrahedron*, **75**, 459 (2019); https://doi.org/10.1016/j.tet.2018.11.075
11. M. Xia, S. Wang and W. Yuan, *Synth. Commun.*, **34**, 3175 (2004); https://doi.org/10.1081/SCC-200028611
12. J. Wantulok, M. Szala, A. Quinto, J.E. Nycz, S. Giannarelli, R. Sokolova, M. Książek and J. Kusz, *Molecules*, **25**, 2053 (2020); https://doi.org/10.3390/molecules25092053
13. A. Tyagi, S. Purohit, P. Oswal, S. Rawat, V. Negi, A.K. Singh and A. Kumar, *New J. Chem.*, **47**, 12511 (2023); https://doi.org/10.1039/D3NJ01341C
14. C. Boulechfar, H. Ferkous, A. Delimi, A. Djedouani, A. Kahlouche, A. Boublia, A.S. Darwish, T. Lemaoui, R. Verma and Y. Benguerba, *Inorg. Chem. Commun.*, **150**, 110451 (2023); https://doi.org/10.1016/j.inoche.2023.110451
15. G.M. Sheldrick, *ActaCryst*, **A64**, 112 (2008); https://doi.org/10.1107/S0108767307043930
16. J. Bernstein, R.E. Davis, L. Shimoni and N.L. Chang, *Angew. Chem. Int. Ed. Engl.*, **34**, 1555 (1995); https://doi.org/10.1002/anie.199515551
17. S. Nagashree, C.S. Karthik, B.L. Sudarshan, L. Mallesha, H.P. Spoorthy, K.R. Sanjay and P. Mallu, *J. Pharm. Res.*, **9**, 509 (2015).
18. S. Poovitha and M. Parani, *BMC Complement. Altern. Med.*, **16(S1)**, 185 (2016); https://doi.org/10.1186/s12906-016-1085-1
19. BIOVIA, Dassault Systèmes, Discovery Studio Visualizer, version 21.1.0.20298, San Diego, CA, USA: Dassault Systèmes (2021).
20. C.E. Satheesh, P. Raghavendra Kumar, P. Sharma, K. Lingaraju, B.S. Palakshamurthy and H. Raja Naika, *Inorg. Chim. Acta*, **442**, 1 (2016); https://doi.org/10.1016/j.ica.2015.11.017
21. C.E. Satheesha, P.R. Kumar, P.A. Suchetan, H. Rajanaika and S. Foro, *Inorg. Chim. Acta*, **515**, 120017 (2021); https://doi.org/10.1016/j.ica.2020.120017
22. M. Salehi, F. Ghasemi, M. Kubicki, M.A. Asadi, M. Behzad, A. Ghasemi and M.H. Gholizadeh, *Inorg. Chim. Acta*, **453**, 238 (2016); https://doi.org/10.1016/j.ica.2016.07.028
23. C.E. Satheesh, P. Raghavendra Kumar, N. Shivakumar, K. Lingaraju, P. Murali Krishna, H. Rajanaika and A. Hosamani, *Inorg. Chim. Acta*, **495**, 118929 (2019); https://doi.org/10.1016/j.ica.2019.05.028